Experimental Approach to Mechanical Property Variability Through a High Density Polyethylene Gas Pipe Wall

ARTICLE *in* JOURNAL OF APPLIED POLYMER SCIENCE · JULY 2005

Impact Factor: 1.77 · DOI: 10.1002/app.21713

4 AUTHORS, INCLUDING:

Lakhdar Boulanouar
Badji Mokhtar - Annaba University
23 PUBLICATIONS **170** CITATIONS
SEE PROFILE

Kamel Chaoui
Badji Mokhtar - Annaba
78 PUBLICATIONS **412** CITATIONS
SEE PROFILE

Experimental Approach to Mechanical Property Variability through a High-Density Polyethylene Gas Pipe Wall

N. Kiass,[1,2] R. Khelif,[2] L. Boulanouar,[2] K. Chaoui[2]

[1]*Physics Department, Badji Mokhtar University, BP 12, Annaba 23000, Algeria*
[2]*Research Laboratory 3MI, Mechanical Engineering Department, Badji Mokhtar University, BP 12, Annaba 23000, Algeria*

Received 11 March 2004; accepted 12 October 2004
DOI 10.1002/app.21713
Published online in Wiley InterScience (www.interscience.wiley.com).

ABSTRACT: An experimental investigation was designed to establish the distribution of mechanical properties throughout a high-density polyethylene (HDPE) gas pipe wall. The proposed approach used a continuous and uniform filament that was automatically machined from the pipe on a precision lathe at a very low cutting speed and an optimal depth of cut to minimize heating and structural disturbances. Typical engineering stress–strain curves, in every layer, were obtained on a testing machine especially designed for polymers, and they were statistically analyzed. The stress–strain behavior of HDPE pipe material could basically be divided into three distinctive zones, the second of which remained important. The average stress level illustrating cold drawing for a given layer was almost constant throughout the pipe wall. The measured stresses and moduli correlated very well with the pipe thickness, and they increased from the outer layers toward the inner layers. This was explained by the crystallinity evolution because the pipe production process was based on a convective water-cooling system with a temperature gradient, which generated residual stresses. Computed statistical stress–strain correlations at yielding, the onset of cold drawing, and fracture points revealed acceptable linear relations for an error level of $p \leq 0.05$. On the other hand, an increasing linear correlation characterized the relationship of the yield stress and elastic modulus. This result was confirmed by literature for standard specimens, prepared by compression molding, that did not represent an actual pipe structure with respect to an extrusion thermomechanical history. Such an approach to mechanical property variability within an HDPE pipe wall highlighted the complexity of the hierarchical structure behavior in terms of stress–strain and long-term brittle failure.
 J Appl Polym Sci 97: 272–281, 2005

Key words: drawing; modulus; orientation; polyethylene (PE); stress

INTRODUCTION

Nowadays, high-density polyethylene (HDPE) resins are commonly processed into pipes and fittings on a large scale to construct natural gas transmission and distribution networks. As shown in recent statistics, more than 90% of newly installed gas systems throughout the world are exclusively made of polyethylene (PE) because of its relatively low cost, ease of installation and maintenance, and long-term durability against environmental degradation; these properties made it a real alternative to metallic systems.[1–5] Despite the large acceptance of PE as an economic alternative, safety remains a basic issue, especially for long-term brittlelike failure and accelerated stress corrosion cracking in both water and gas piping systems. It is possible to control to a certain extent the physical properties of semicrystalline polymers by morphology management during processing operations.[6–13] Substantially improved Young's moduli and tensile strengths have been obtained in shear-controlled orientation in injection-molded and high-pressure injection-molded HDPE because of the appearance of highly oriented structures.[14] Quasi-static mechanical testing of HDPE processed by shear controlled orientation in injection molding (SCORIM) exhibited an improvement of 59% in the flexural modulus in comparison with the mechanical performance of conventional injection-molded specimens.[15] For extruded pipes, the residual stresses and morphology variations are primarily due to the fabrication process, which does not allow progressive heat dissipation.[15–18] The search for homogeneous geometrical dimensions in terms of the diameter and wall thickness, which are represented by the standard dimension ratio (SDR), imposes rapid cooling. Consequently, compressive stresses in the extrusion process are generated on external pipe layers, whereas the internal layers develop positive stresses. The resistance to crack propagation is amply influenced by the state and magnitude of these residual stresses. Moreover, it has been shown that the propagation of cracks is slower in the external layers when they are subjected to compressive residual stresses.[19]

Correspondence to: K. Chaoui (chaoui_k@wissal.dz).
Contract grant sponsor: Sonatrach Oil Co.; contract grant number: D6001 Z.

Another important issue is slow crack growth (SCG) because PE pipe materials exhibit stress/time-to-failure curves that have two separate rates corresponding to both ductile and brittle fracture mechanisms, that is, knee-type curves. The long-term behavior associated with brittlelike failure is most feared because it takes place without any presaging signs. At the same time, the long-term strength is substantially reduced, and so linear predictions from short-term behavior are no longer applicable. As a result, appropriate test designs have been developed to study crack propagation in real pipe materials under creep and fatigue modes and to figure out correlations between various mechanisms.[3–5,16,20–27] Using a fatigue crack propagation mode at a maximum stress intensity factor $K_{I\max} = 1.3$ MPa and a load ratio $R = 0.1$, researchers have identified basic differences in the damage zone between HDPE and medium-density polyethylene (MDPE) pipe resins with scanning electron microscopy examinations.[28] Those observations are critical because the damage zone represents sites at which most hierarchical events happen and automatically controls the crack growth rate. Subsequently, this control defines the ultimate resistance to long-term fracture. Knowing that most of the pipe lifetime is controlled by the initiation period and having identified the notch root damage zone, researchers have become interested in single and epsilon-shaped crazes in HDPE and MDPE pipe materials, respectively. The corresponding morphologies reveal drastic differences in the organization of the highly drawn material. Although a single HDPE craze accommodates uniaxially drawn fibrils, the multiple MDPE craze is solely made of voids and biaxially stretched planes.[21,25,28]

At this stage, we need to correlate the usual mechanical properties, measured macroscopically, with the associated structure of pipe resins. In other words, there is a need to explain the physical and mechanical properties of pipe materials with respect to the molecular architecture and viscoelastic behavior.[10,11,15] Brittle failure in semicrystalline polymers has been claimed to originate from chain disentanglement in fibrils, and recently other studies have also concluded that chain breaking due to applied stress during crack propagation involves fibrillation within the damage zone.[19,20,22,27,29] A level of complexity lies in the intramolecular heterogeneity of counit distribution that should be as efficient as intermolecular heterogeneity for producing tie molecules and random chain folding at the expense of regular chain folding.[6,11] Crystalline domains within semicrystalline polymers strongly influence such low-strain-rate properties as the elastic modulus (E), yield stress (σ_y), SCG, and environmental stress cracking, whereas high-strain-rate properties such as impact, tear, and rapid crack propagation are basically controlled by amorphous regions.[30,31] In many cases, complementary techniques have been adopted to assess from physical property measurements molecular information. For instance, brittle fracture toughness, crazing, and SCG measurements have been used to determine the tie-molecule concentration and to infer valuable structural information.[32] In simpler cases, tie-molecule concentrations have been evaluated from the modulus of a mechanically oriented material. Postyield experiments assume that tie molecules and entangled chains behave like rubbery networks in the drawing and strain-hardening regions; these molecules are steadily pulled out from fragmented lamellae to become part of an oriented amorphous domain.[11] The mechanical properties of plastic pipes are also affected by the morphology of the matter. For example, the mechanical resistance of a polymer depends on the rigidity of the chains and on the concentration of the intracrystalline and intercrystalline molecular segments that provide the load-bearing strength of the bulk polymer. This resistance is deeply affected by the processing and service temperatures during the transmission of pressurized gas. Consequently, both the vitreous transition and fusion temperature become significant parameters that condition the employment and working opportunities of HDPE pipes. Piping material must be reinforced in two directions circumferentially to improve its ability to sustain pressure and to longitudinally preserve both mechanical resistance and toughness sufficient to handle external loads. In most relevant equations, geometrical dimensions such as the outside diameter (OD) and thickness (h) are related to the mechanical properties for plastic pipes. For instance, as shown in French Standard NF EN 921 for pressurized plastic pipe tests, the hoop stress (σ_{hoop}) can be calculated from the Lamé relationship:[3]

$$\sigma_{\text{hoop}} = P\,\frac{\text{OD} - h}{2h} \tag{1}$$

where P is the absolute internal pressure. On the other hand, for the calculation of the maximum residual stress ($\sigma_{\max}$) in plastic pipes, the following relation is an approximation involving the creep modulus at time t [$E(t)$] and the pipe thickness:[33]

$$\sigma_{\max} = \frac{\pm\, E(t)h}{1 - \nu^2}\,\frac{D_2(t) - D_1}{D_2(t)D_1} \tag{2}$$

where D_1 and D_2 are pipe diameters before and after ring slitting and ν is the Poisson's ratio. Alternatively, the stress acting on the pipe wall (σ) should obey an equation of the following form to ensure safe working conditions:[34]

$$\sigma^2 \geq \frac{2(K_c)^2(1 - \nu^2)}{\pi D} \tag{3}$$

where D is the average diameter and K_c is the material fracture toughness. Now, the other step is designing experiments for HDPE pipes for the purpose of investigating mechanical property correlations with morphology parameters such as the crystallinity (X), molecular weight (M_0), and average number of segments in the average tie chain (N). Schultz[35] reported that Krigbaum et al. succeeded in deriving and applying a useful expression for the initial E value of a deforming spherulitic polymer:

$$E = \frac{\rho RT}{M_0}\left[\frac{1}{5}\frac{1}{N(1-X)^3}\frac{\beta^2\sinh\beta}{\sinh\beta-\beta^2}+\frac{4}{5}\frac{\beta}{N^{1/2}(1-X)}\right] \quad (4)$$

where ρ is the material density, T is the absolute temperature, and R the universal gas constant. The parameter β is calculated as follows:

$$\frac{\sinh\beta}{\beta} = \exp\left[\frac{\Delta H_f}{R}\left(\frac{1}{T}-\frac{1}{T_m^0}\right)\right] \quad (5)$$

where ΔH_f is the heat of fusion per unit volume and T_m^0 is the melting temperature at equilibrium. Using such a relation, the direct influence of the morphology from X, N, and ρ on the mechanical properties can be appreciated. Interestingly, another approach was created to estimate the chain-direction modulus of a polymer crystallizing with its backbone in the form of a planar zigzag as the deformations involve only the bending and stretching of the bonds. For a polymer consisting of n rods, each of length l and joined together by torsional springs, if θ is the bond angle and A is the cross-sectional area supported by each chain, then E can be derived as follows:[36]

$$E = \frac{l\,\sin(\theta/2)}{A}\left[\frac{\sin(\theta/2)}{k_1}+\frac{l^2\cos^2(\theta/2)}{4k_0}\right]^{-1} \quad (6)$$

where k_l and k_θ are the bond stretching and angular deformation force constants, respectively. However, simpler approaches are sought for the immediate analysis of plastic pipes.

In this study, we attempted to design a simple experimental procedure to establish the distribution of mechanical properties throughout an HDPE pipe wall. The idea consists of preparing specimens as a function of the layer position within the pipe shell, showing that they are consistent for the measurement of the mechanical properties in a reproducible manner, and then constructing correlations about pipe heterogeneity due to thermomechanical effects. Because both the production and usage of HDPE pipes involve heat generation to form and weld pipe sections, morphology variances and stress gradients will exist in various manners and will influence differently pipe resins during their service life. As a result, figuring out and understanding the evolution of the mechanical properties within the pipe itself and correlating the final results to the morphology and eventually to the residual stresses were set as the objectives for this work.

EXPERIMENTAL

Material

The material used in this study was an HDPE pipe extruded from a Europlast PE 80 resin (MTG-Sonelgaz, Oran, Algeria) in conformity with the general quality requirements and testing stated in DIN 8075. According to ISO 9080, the minimum required strength for this resin is 6.3–8 MPa for a 50-year safe service period. The melt flow index and density of the pigmented pipe material were 0.9 and 0.954, respectively. Sonelgaz, the Algerian national electricity and gas company, generously supplied pipe specimens, with an external average OD of 125 mm and an average wall thickness of 11.4 mm (SDR 11). This piping material is used in relatively moderate climates at an average gauge pressure of 4 bars and is subjected to a normalized 6 bars of effective hydraulic testing pressure.

Specimen preparation

To measure the mechanical properties in every layer within the cylinder, we needed to prepare specimens with the following criteria: (1) the specimens should be directly extracted from the pipe to conserve the intrinsic thermomechanical history, (2) they should obey a reproducible preparation methodology, and (3) structural morphology disturbances should be kept to a minimum through the reduction of contact stresses during the automatic machining operation. Several cutting conditions were tried with a machining program to obtain the most regular filament section for a through wall turning. A fitted wooden mandrel was fabricated to support internally the pipe and three large metallic bearings, which uniformly distributed the clamping stresses on the pipe's outer surface. Thus, the lathe spindle firmly held both the pipe and mandrel without damaging the clamped pipe portion. To avoid any radial displacement of the revolving assemblage, the mandrel was also supported by a headstock. Filament cutting was performed continuously in the radial direction with a 2-mm-thick carbon steel right tool at a low spinning speed of 45 rpm. To keep the cutting forces to a low level, the cut depth was chosen to be 0.5 mm; because the machining was orthogonal, there was no need for a feed rate or an outside cooling medium. A microscopic examination permitted us to verify the global uniformity of the filament and the rectangular cross-sectional area. The machining operation could induce some stresses due to cutting and also relieve others; however, because

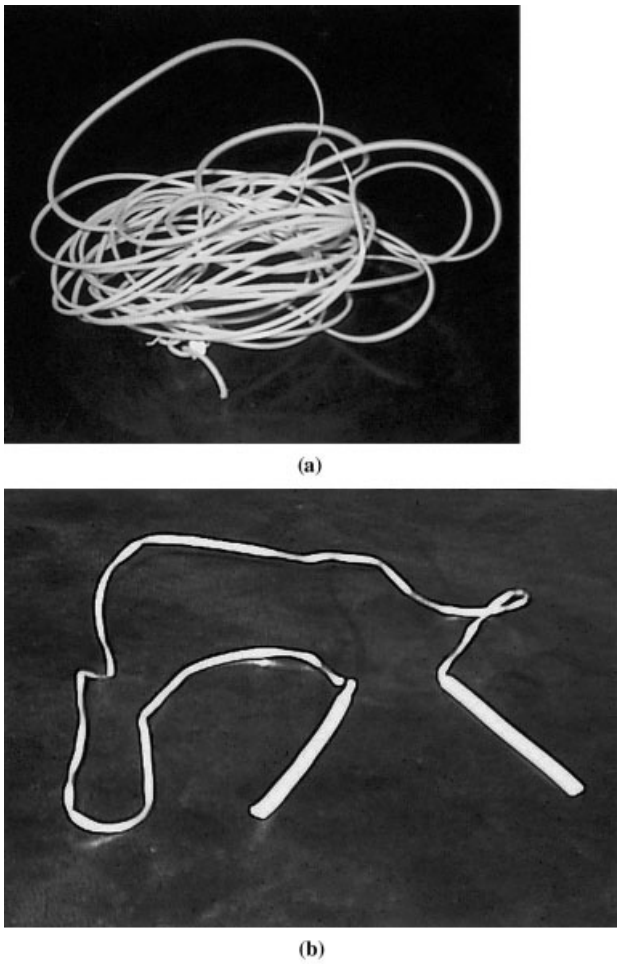

Figure 1 (a) HDPE filament machined at a low speed from the pipe wall in the inward direction and (b) the specimen tested under uniaxial tension until the breaking point.

the objective was comparison, all the specimens were prepared in a single operation under exactly the same conditions. One whole filament allowed the preparation of at least 50 specimens, each 150 mm long (Fig. 1). Each specimen was identified geometrically and spatially within the pipe wall with respect to the initial cylinder with a volumetric approach.[37]

Experimental procedure

The filament specimens were subjected to monotonic tensile loads with a Zwick/Roell Materialprüfung Zwicki 1120 universal testing machine (Ulm, Germany) especially designed for polymer characterization with a 2-kN load cell. A 1.66 mm/s testing speed was used, and the setup was monitored with a computer program that allowed carrying out all tests in exactly the same way on the basis of the general recommendations of ASTM D 638. To obtain the final failure of the filament, the gauge length was reduced from 64 to 40 mm to accommodate the specimen geometry with the machine's maximum crosshead displacement; such a length was also reported in the literature.[38] The TestXpert software (Technosid/Zwick, Annaba, Algeria) controlled the experimental output data and recorded the checked information in real time through an RS232 computer interface. Instantaneous statistical analysis was performed on request during every data acquisition according to a testing program previously declared to the software. This step ensured calculating the means and standard deviations for each set of specimens that belonged to the same HDPE layer and constructed the average engineering stress–strain curve for a given dimensionless pipe thickness, as shown in Figure 2. A total of 109 tests were carried out at the ambient temperature for two identically prepared lots (lot 1 and lot 2).

RESULTS

Figure 2 illustrates a typical stress–strain curve delivered by the TestXpert software report for a layer composed in this case of three specimens. Three distinctive zones characterized the behavior: (1) a linear elastic region, (2) a cold-drawing region enclosed between points A and B (which has for this layer over 500% strain), and (3) an ultimate material tearing coupled with failure. This curve intrinsically identifies the behavior of semicrystalline polymers, which are normally more ductile, especially between the glass-transition temperature and the melting temperature, and undergo cold drawing before ultimate failure. Careful observations indicated that cold drawing was initiated just after the yield point and before point A (Fig. 2). After point B, strain hardening took place, and the stress rose until crystal blocks became aligned parallel

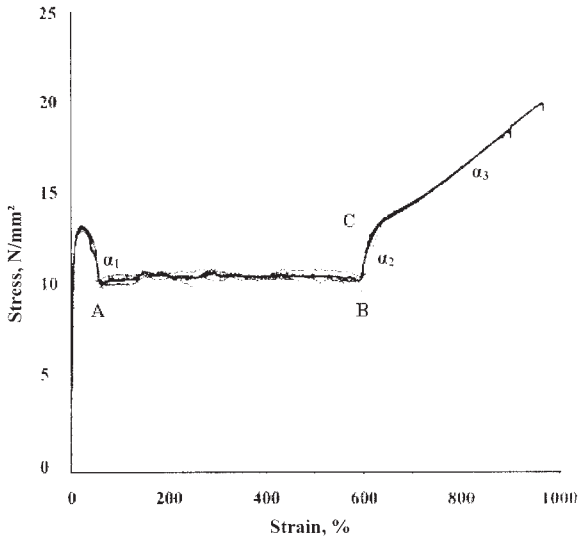

Figure 2 Engineering stress–strain curves, obtained with TestXpert software, for a set of HDPE filaments belonging to the same pipe layer. The bold curve is the instantaneous statistical average.

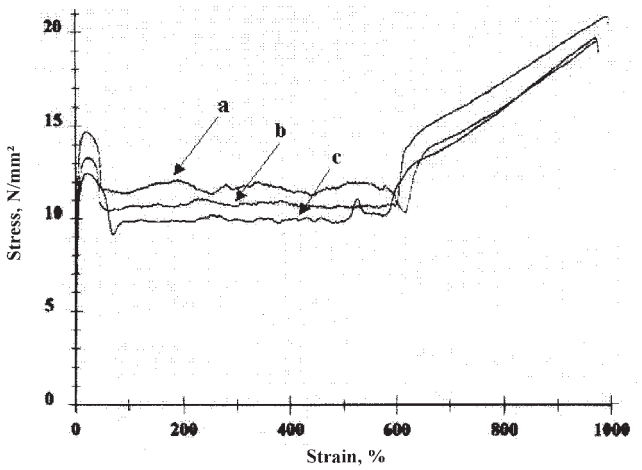

Figure 3 Comparison of typical engineering stress–strain curves for (a) outermost, (b) middle, and (c) innermost layers of an HDPE pipe.

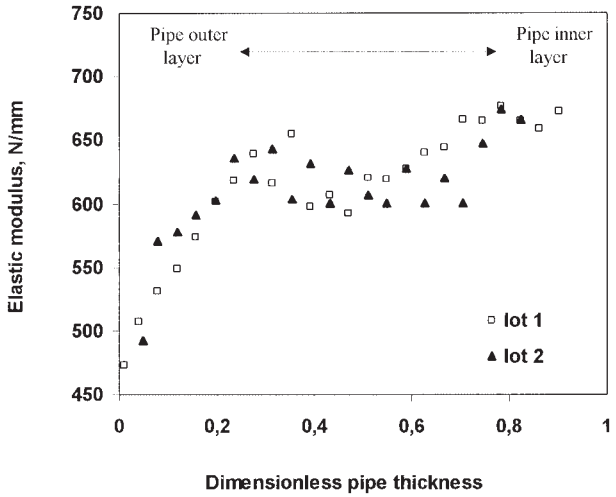

Figure 4 Variation of E through an HDPE gas pipe wall for two identical lots.

to the stretching direction when a fibrillar structure was formed.[35–38] To highlight variances within the pipe wall, a comparison of stress–strain curves at the outermost, middle, and innermost positions proved that the general trend was very similar, and the three observed zones were preserved; however, the identifying points were completely displaced. Additionally, a trend was being followed as the measurements moved from the inner layer toward the outer one (Figs. 2 and 3). To study this variability, the usual mechanical properties were recorded, and others were requested for calculation through the TestXpert software for each shell layer.

For E and σ_y (Figs. 4 and 5), there were clear increases from the inner pipe layers to the outer pipe layers, and within the region between 30 and 70% of the pipe thickness, a plateau was observed; it probably indicated a zone that was not readily affected by transient heat transfer during extrusion, especially for pipes obtained from the melt and rapidly water-cooled from the external surface.[37] On the other hand, the inner surface had enough time to cool down by free convection. As we inferred from the previous equations, this thermal state conditioned both the E and σ_y behaviors. Most equations predict an increase in E and σ_y with X, but in this instance, it should be emphasized that the cylinder case is different as there is a temperature gradient that controls the transient thermodynamic system during cooling. This deduction is mostly true for the lamellar averaging scheme of Boyd and the semiempirical Tsai–Halpin equation.[35,36,39–41] It is possible with the obtained data to write the following polynomial equations that express E and σ_y distributions throughout the pipe wall:

$$E = 1349.80\left(\frac{t}{t_0}\right)^3 - 2002.70\left(\frac{t}{t_0}\right)^2 + 960.87\left(\frac{t}{t_0}\right) + 475.75 \quad (R^2 = 0.83) \quad (7)$$

$$\sigma_y = 15.55\left(\frac{t}{t_0}\right)^3 - 23.80\left(\frac{t}{t_0}\right)^2 + 12.49\left(\frac{t}{t_0}\right) + 11.53 \quad (R^2 = 0.75) \quad (8)$$

with t_0 the initial thickness in mm and R^2 the coefficient of determination. Figure 6 presents a similar observation for the nominal cold-drawing stress (σ_{CD}) because it also increased in the inward pipe radial direction. The calculated mean and standard deviation were 10.73 and 0.53 N/mm^2, respectively, for both lots, and this indicated a consistency in measurements and emphasized a corresponding structural hierarchy most likely controlled by X during the constant volume flow process. In a similar manner, the average cold-drawing stress ($\bar{\sigma}_{CD}$) was followed through the pipe thickness and was found to obey the following relation:

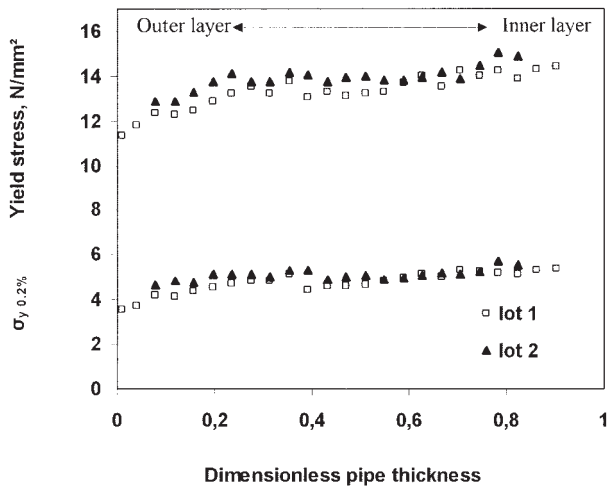

Figure 5 Comparison of $\sigma_{y0.2\%}$ and σ_y variations through a pipe wall for two identical lots.

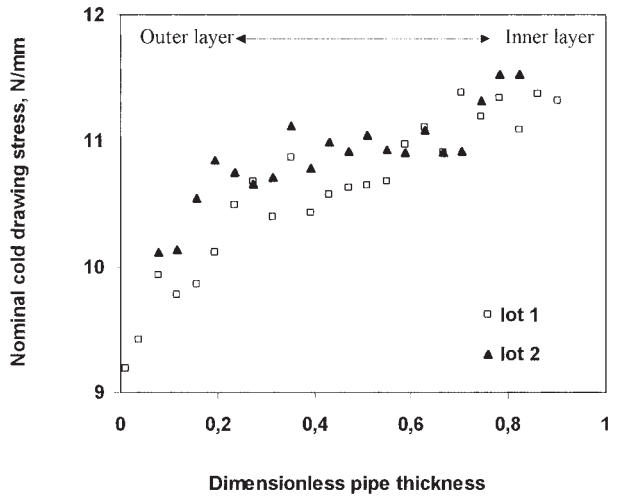

Figure 6 Evolution of the nominal σ_{CD} values as a function of the pipe wall.

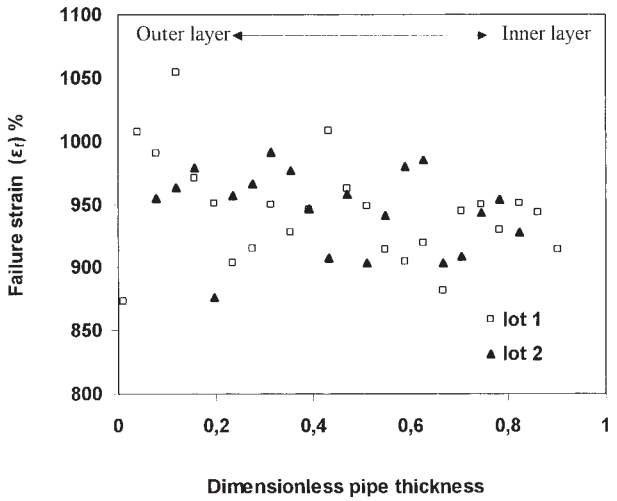

Figure 8 Variation of the measured ε_f values (%) as a function of the pipe wall thickness.

$$\overline{\sigma_{CD}} = 8.47\left(\frac{t}{t_0}\right)^3 - 13.53\left(\frac{t}{t_0}\right)^2 + 7.85\left(\frac{t}{t_0}\right) + 9.28 \quad (R^2 = 0.84) \quad (9)$$

For strain measurements, the correlations were not obvious for the yield strain (ε_y) and failure strain (ε_f; Figs. 7 and 8). Strain dispersions throughout the pipe thickness were important, but the reproducibility was maintained for ε_y and ε_f as lots 1 and 2 confirmed such variances. The extent of cold drawing (%) is presented in Figure 9. Lower measured values occurred at the pipe bore, and beyond the 20% thickness limit, appreciable dispersion was revealed for both lots within the range (480–580%). In the second zone, cold drawing occurred through two mechanisms. In the first case, drawing began in the middle span at only one site, and the neck propagated steadily toward the grips. Alternatively, in other cases, the onset of drawing was characterized by multiple necking locations independently evolving and then merging together. During this process, zooming into the real-time stress–strain curve showed characteristic localized fluctuations that described the associated drawing activity. Although plastic flow took place, the crystallites became deformed plastically and underwent plastic shearing localized in slip planes.

The plastic hardening was ascribed not only to a weak share of crystalline plasticity consolidation but also to the strong entropic effects of the molecular orientation in the amorphous phase and then in the crystallites themselves. For large plastic deformations, the chains also underwent a progressive orientation, and so their later distortion became increasingly difficult. This required an increase in the strain-harden-

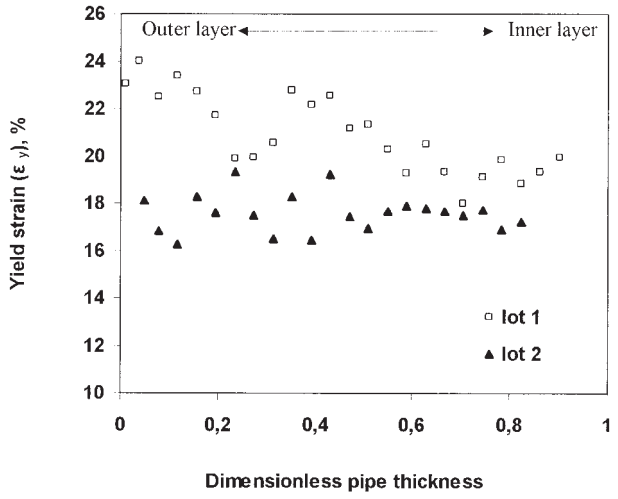

Figure 7 Variation of the measured ε_y values (%) as a function of the pipe wall thickness.

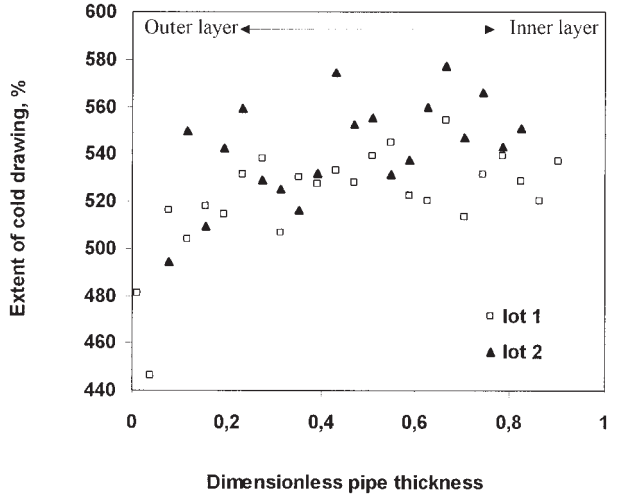

Figure 9 Measured extent of cold drawing through the pipe wall thickness.

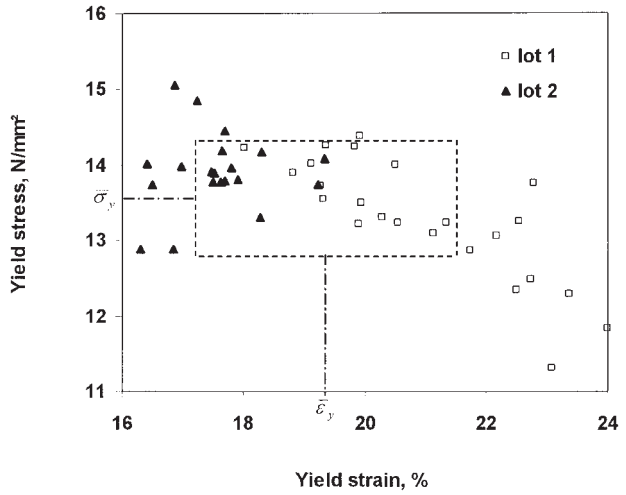

Figure 10 Relationship between the measured σ_y and ε_y values ($\bar{\sigma}_y$ and $\bar{\varepsilon}_y$ are the average values, and the enclosed area represents variations within two standard deviations).

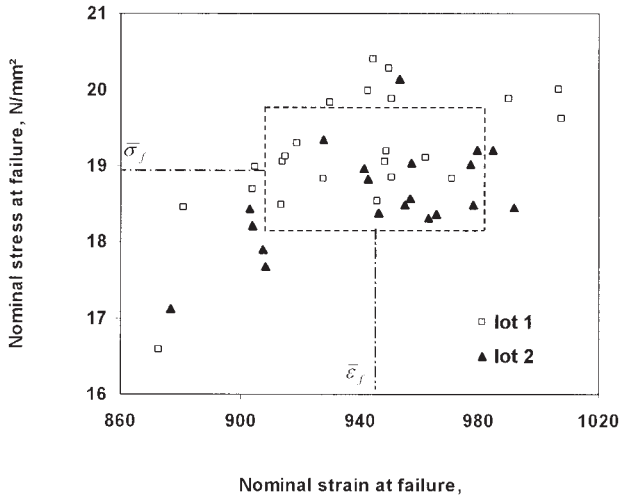

Figure 12 Relationship between the nominal σ_f and ε_f values ($\bar{\sigma}_f$ and $\bar{\varepsilon}_f$ are the average values, and the enclosed area represents variations within two standard deviations).

ing stress, and the crystallites finally split into a strongly anisotropic fibrous texture oriented in the direction of traction. Final fiber rupture occurred by large-scale deformations and locally cracked fibers.[35,38,42]

Statistical analysis was carried out with the obtained data to validate the trends and to examine whether significant differences existed between the tested lots. All data were as subjected to normal distribution, and the dispersion around the mean was analyzed. Three characteristic points represented by σ_y and ε_y, the onset of drawing (point A in Fig. 2), and the failure point [the failure stress (σ_f) and ε_f] are presented. The mean values and standard deviations were calculated and are shown in Figures 10–12. The zone formed by dashed lines enclosed two standard deviations around the mean value and was set to estimate the constancy by the calculation of the percentage of points within the area. The obtained values were 62, 57, and 56% from Figures 10–12, respectively, and this indicated that approximately more than half of the obtained data for these three points supported an acceptable normal distribution.

Besides E, three other slopes (α_1, α_2, and α_3) were measured, as shown in Figure 2. α_1 describes the portion of the stress–strain curve bounded by σ_y and the onset σ_{CD} value (point A), whereas α_2 and α_3 illustrate the strain hardening between points B and C and the ultimate fully drawn material till final failure, respectively. The results are listed in Table I. α_1 was in

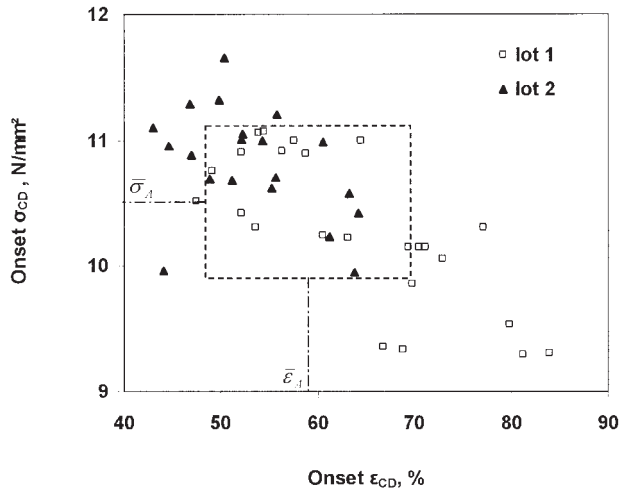

Figure 11 Relationship between the measured onset σ_{CD} and ε_{CD} values (see point A in Fig. 2; $\bar{\sigma}_A$ and $\bar{\varepsilon}_A$ are the average values, and the enclosed area represents variations within two standard deviations).

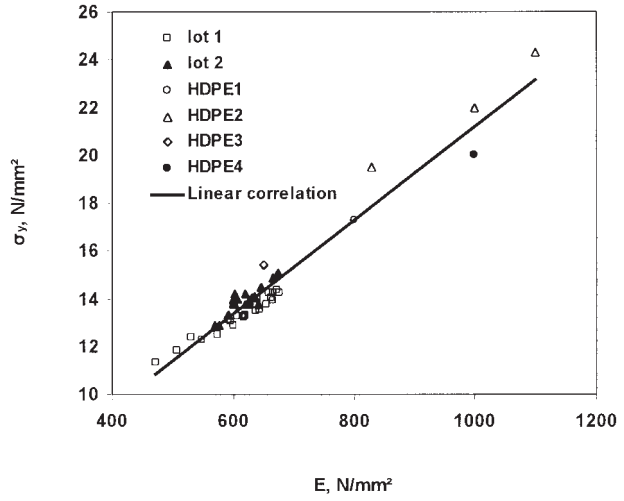

Figure 13 Relationship between σ_y and E in comparison with compression-molded literature data (HDPE1, M_w/M_n = 1.19; HDPE2, M_w/M_n = 1.19, quenched in ice; HDPE3, M_w/M_n = 2.89; slowly cooled, ref. 48; and HDPE4, ref. 50).

TABLE I
Variations of the Slopes α_1, α_2, and α_3 as Illustrated in Figure 2 Throughout the Pipe Wall

	$\left(\frac{t}{t_0}\right)$								
	0.12	0.20	0.31	0.39	0.51	0.59	0.71	0.82	0.90
α_1	−0.053	−0.060	−0.070	−0.060	−0.070	−0.080	−0.094	−0.097	−0.096
α_2	0.160	0.194	0.111	0.157	0.119	0.071	0.116	0.149	0.127
α_3	0.019	0.019	0.020	0.018	0.019	0.020	0.020	0.019	0.018

relative progression; this means that stress falling and necking occurred at an increasing local speed because the slope was steeper as a function of the pipe wall thickness. As expected, α_3 exhibited a roughly constant value for fully drawn fibers beyond C when all chains were extended to the maximum. No specific correlation was observed for slope α_2 as it probably constituted the search for a thermodynamic equilibrium condition preceding the state of fully drawn fibers.

DISCUSSION

The observed stress–strain behavior is also reported in the literature for different specimen geometries.[35,38,39,43–46] The use of compression-molded specimens may not exactly reproduce the pipe structure, at least in terms of residual stresses; in addition, preparing standard ASTM specimens from the pipe involves lengthy operations of cutting and machining through the wall, which will disturb the initial morphology. In pursuit of similar objectives, engineering stress–strain curves of standard specimens were also used to establish fine differences in E, σ_y and ε_f among butt-fusion specimens, electrofusion specimens, and plain, unwelded counterparts.[44] In common with this study, it was observed that the ultimate tensile stress exhibited a trend similar to that of E (Figs. 4 and 5), with electrofusion being inferior in all cases. Because thicker pipes are sought for higher flow rates and increased network pressures, the influence of the plastic pipe joining method is another major variable that ought to be investigated separately, and the approach described here would be appropriate. This is a crucial issue for long-term behavior as the welded specimens exhibited lower tensile properties. For flow-formed HDPE pipes, structurally altered specimens were produced, and the mechanical properties were studied as a function of the diameter reduction percentage. On the basis of ASTM Standards D 2105 and D 1599, less yielding and cold drawing were revealed as the reduction percentage increased, whereas in the axial and hoop directions, toughness improvement was confirmed.[45] Furthermore, X measurements were performed on MDPE and HDPE pipe materials, and it was concluded that up to an 8% difference existed between the outer and inner layers. In fact, X increased through the pipe wall from the innermost surface toward the external layer.[47] Besides, it was concluded that the life predicted from constant tensile load (CTL) tests increased linearly with average X. These results supported the findings of this study, as shown in Figures 3–6. Correlations involving strains (ε_y, ε_f, and the extent of cold drawing) did not show linear trends, as stated in Table II, according to statistical analysis carried out with all the data with Statistica software (version 5.1). The goodness of fit was tested with the Fisher–Snedecor test for a preset probabilistic error level of $p \leq 0.05$. The accepted correlations are shown with an asterisk in Table II.

To confirm the usefulness of the approach with statistical analysis, we observed that both E and σ_y correlated very well with increasing pipe wall thickness. Consequently, a plot of σ_y as a function of E was constructed and compared with data from the literature (Fig. 13). We concluded that the linear relationship between these two mechanical properties was preserved in this approach and compared quite well with others' data.[48–50] The correlation governing this relationship for PE 80 is

$$\sigma_y = 0.0196E + 1.5575 \quad (R^2 = 0.95) \qquad (10)$$

For the testing conditions adopted here, both σ_y and E should normally reflect X.[35,36,48–50] σ_y increased with the hydrostatic pressure, and this resulted simultaneously in an increase in both the shear modulus and Young's modulus. In addition, as σ_y increased with the plastic strain, which produced a growth in orientation, E was also augmented, and this dependence has been reported in some works.[51–54] Besides structural effects, the variability of the mechanical properties within the pipe wall should be integrated as new evidence to assess the long-term strength and be closely correlated with internal stresses, which may play another role as outer compressive residual stresses contributing to strengthening, whereas positive stresses are to be overcome beyond approximately half the pipe thickness.

CONCLUSIONS

This study allowed us to investigate the distribution of common mechanical properties throughout an HDPE gas pipe wall. The experimental approach was set to

TABLE II
Determination Coefficients and p Values Between Selected Variables as a Function of Pipe Wall Thickness

	Position	E	σ_y 0.2%	σ_y	σ_{CD}	σ_f	ε_y	ε_f	Cold-drawing Extent	A stress	A strain	B stress	B strain	C stress
E	0.772*	—												
	$p = 0.0001$													
σ_y0.2%	0.725*	0.881*	—											
	$p = 0.0005$	$p = 0.0000$												
σ_y	0.784*	0.878*	0.972*	—										
	$p = 0.0004$	$p = 0.0007$	$p = 0.0000$											
σ_{CD}	0.861*	0.886*	0.929*	0.967*	—									
	$p = 0.0000$	$p = 0.0005$	$p = 0.0000$	$p = 0.0000$										
σ_f	0.343*	0.334*	0.151	0.199	0.249	—								
	$p = 0.0223$	$p = 0.0273$	$p = 0.3271$	$p = 0.1968$	$p = 0.1029$									
ε_y	−0.358*	−0.453*	−0.718*	−0.669*	−0.589*	0.190	—							
	$p = 0.0177$	$p = 0.0022$	$p = 0.0008$	$p = 0.0009$	$p = 0.0009$	$p = 0.2170$								
ε_f	−0.284	−0.224	−0.253	−0.232	−0.281	0.565*	0.200	—						
	$p = 0.0624$	$p = 0.1444$	$p = 0.0982$	$p = 0.1301$	$p = 0.0651$	$p = 0.0004$	$p = 0.1930$							
Cold-drawing extent	0.503*	0.538*	0.623*	0.645*	0.632*	−0.206	−0.511*	−0.349*	—					
	$p = 0.0003$	$p = 0.0008$	$p = 0.0003$	$p = 0.0005$	$p = 0.0002$	$p = 0.1796$	$p = 0.0001$	$p = 0.0208$						
A stress	0.798*	0.754*	0.896*	0.927*	0.915*	0.040	−0.696*	−0.376*	0.674*	—				
	$p = 0.0007$	$p = 0.0004$	$p = 0.0005$	$p = 0.0000$	$p = 0.0000$	$p = 0.7950$	$p = 0.0006$	$p = 0.0125$	$p = 0.0003$					
A strain	−0.484*	−0.453*	−0.647*	−0.642*	−0.638*	0.208	0.732*	0.479*	−0.710*	−0.731*	—			
	$p = 0.0014$	$p = 0.0022$	$p = 0.0006$	$p = 0.0001$	$p = 0.0007$	$p = 0.1767$	$p = 0.0002$	$p = 0.0018$	$p = 0.0009$	$p = 0.0001$				
B stress	0.802*	0.778*	0.820*	0.854*	0.881*	0.311*	−0.498*	−0.233	0.564*	0.845*	−0.518*	—		
	$p = 0.0001$	$p = 0.0007$	$p = 0.0000$	$p = 0.0004$	$p = 0.0000$	$p = 0.0401$	$p = 0.0018$	$p = 0.1283$	$p = 0.0004$	$p = 0.0004$	$p = 0.0007$			
B strain	0.385*	0.450*	0.450*	0.482*	0.467*	−0.152	−0.252	−0.184	0.912*	0.468*	−0.360*	0.447*	—	
	$p = 0.0105$	$p = 0.0020$	$p = 0.0020$	$p = 0.0012$	$p = 0.0016$	$p = 0.3232$	$p = 0.0992$	$p = 0.2323$	$p = 0.0000$	$p = 0.0018$	$p = 0.0169$	$p = 0.0027$		
C stress	0.817*	0.823*	0.834*	0.886*	0.914*	0.272	−0.528*	−0.286	0.715*	0.823*	−0.606*	0.867*	0.595*	—
	$p = 0.0006$	$p = 0.0003$	$p = 0.0003$	$p = 0.0005$	$p = 0.0000$	$p = 0.0742$	$p = 0.0008$	$p = 0.0606$	$p = 0.0004$	$p = 0.0002$	$p = 0.0006$	$p = 0.0006$	$p = 0.0004$	
C strain	0.428*	0.468*	0.542*	0.595*	0.557*	−0.111	−0.424*	−0.177	0.923*	0.570*	−0.521*	0.550*	0.920*	0.716*
	$p = 0.0047$	$p = 0.0017$	$p = 0.0002$	$p = 0.0005$	$p = 0.0006$	$p = 0.4740$	$p = 0.0044$	$p = 0.2516$	$p = 0.0000$	$p = 0.0009$	$p = 0.0001$	$p = 0.0009$	$p = 0.0000$	$p = 0.0006$

An asterisk indicates statistically accepted error level.

determine mechanical properties and to quantify local differences. Although the specimens were prepared from a continuous filament obtained in a one-step machining operation, the results were in good agreement with those of the literature. The properties representing stresses increased from outer layers toward inner layers. This was explained by the evolution of X because the fabrication process involved cooling at differential temperature gradients and thus generated residual stresses. In terms of strains, the trends were not quite obvious, but there was a tendency for some dispersion. The obtained stress–strain correlations within the pipe wall at yielding and the onset of cold-drawing points indicated a decreasing linear relation. On the other hand, the σ_y relation with E was characterized by an increasing linear correlation. The variability of the mechanical properties within the pipe wall revealed the complexity of the hierarchical structure in HDPE, and such an approach is intended to contribute to our understanding of the long-term behavior and associated brittle failure of pipes.

The authors are grateful to Sonelgaz Co. for providing high-density polyethylene pipe samples. The experimental program was carried out at the Laboratoire de Recherche en Mécanique des Matériaux et Maintenance Industrielle (LR3MI) and was authorized by decree MESRS 42/2001.

References

1. Gas Research Institute. Pipeline Statistics, Distribution and Transmission, Annual Mileage Totals, Chicago, 2002. http://www.gri.org/pub (accessed January 2002).
2. Cheron, J. J. Pipeline Gas Ind 2001, 84, 5.
3. Boot, G. C.; Toropova, I. L. Trenchless Technol Res 1999, 14, 13.
4. Hamouda, H. B. H.; Somoes-betbeder, M.; Grillon, F.; Blouet, P.; Billon, N.; Piques, R. Polymer 2001, 42, 5425.
5. Munier, C.; Gaillard-Devaux, E.; Tcharkhtchi, A.; Verdu, J. J Mater Sci 2002, 37, 4159.
6. Kalay, G.; Sousa, R. A.; Reis, R. L.; Cunha, A. M.; Bevis, M. J. J Appl Polym Sci 1999, 73, 2473.
7. Keller, A.; Kolnaar, H. Mater Sci Technol 1997, 18, 191.
8. Kalay, G.; Allan, P. S.; Bevis, M. J. Kunststoffe 1997, 35, 241.
9. Doroudiani, S.; Park, C. B.; Kortschot, M. T. Polym Eng Sci 1998, 38, 1205.
10. Janimak, J. J.; Stevens, G. C. J Mater Sci 2001, 36, 1879.
11. Hubert, L.; David, L.; Séguéla, R.; Vigier, G.; Degoulet, C.; Germain, Y. Polymer 2001, 42, 8425.
12. Pan, S. J.; Brown, H. R.; Hiltner, A.; Baer, E. Polym Eng Sci 1987, 27, 869.
13. Aubert, A.; G'Sell, C.; Dahoun, A.; Dargent, E.; Grenet, J. Rev Métall Cahiers Inf Tech 1999, 12, 1511.
14. Ogbonna, C. I.; Kalay, G.; Allan, P. S.; Bevis, M. J. J Appl Polym Sci 1995, 58, 2131.
15. Mano, J. F.; Sousa, R. A.; Reis, R. L.; Cunha, A. M.; Bevis, M. J. Polymer 2001, 42, 6187.
16. Boot, G. C.; Guan, Z. W.; Toropova, I. Trenchless Technol Res 1996, 11, 37.
17. Chaoui, K.; Moet, A.; Chudnovsky, A. In Recent Advances in Experimental Mechanics; Proceedings of the 10th International Conference on Experimental Mechanics; Lisbon, Portugal, Silva Gomez, J. F.; Branco, F. B.; Martins de Brito, F.; Soussa Cirne, J.; Correira da Cruz, A.; Gil Saraiva, J.; Lurdes Eusébio, M., Eds.; A. A. Balkema, Rotterdam, Netherlands Brookfield, VT, 1994; p 811.
18. William, J. G.; Hodgkinson, J. M.; Gray, A. Polym Eng Sci 1981, 21, 822.
19. Chaoui, K.; Moet, A.; Chudnovsky, A. J Mater Sci 1987, 22, 3879.
20. Brown, N.; Lu, X.; Huang, Y.-L.; Qian, R. Macromol Chem 1995, 41, 55.
21. Chaoui, K. J Mater Sci Lett 1989, 8, 326.
22. Shah, A.; Stepanov, E. V.; Hiltner, A.; Baer, E.; Klein, M. Int J Fract 1997, 84, 159.
23. Parsons, M.; Stepanov, E. V.; Hiltner, A.; Baer, E. J Mater Sci 2000, 35, 1857.
24. Kadota, K.; Chum, S.; Chudnovsky, A. J Appl Polym Sci 1993, 49, 863.
25. Strebel, J.; Chaoui, K.; Chudnovsky, A.; Moet, A. Presented at the International Gas Research Conference, Tokyo, Japan, 1989; Paper 218B.
26. Reynolds, P. T.; Lawrence, C. C. J Mater Sci 1991, 26, 6197.
27. Plummer, C. J. G.; Goldberg, A.; Ghanem, A. Polymer 2001, 42, 9551.
28. Parsons, M.; Stepanov, E. V.; Hiltner, A.; Baer, E. J Mater Sci 2001, 36, 5747.
29. Plummer, C. J. G.; Scaramuzzino, P.; Kaush, H. H. Polym Eng Sci 2000, 40, 1306.
30. Yeh, J. T.; Chen, J. H.; Hong, H. S. J Appl Polym Sci 1994, 54, 2171.
31. Yeh, J. T.; Runt, J. J Polym Sci Part B: Polym Phys 1991, 29, 371.
32. Ishikawa, M.; Ushui, K.; Kondo, Y.; Hatada, K.; Gima, S. Polymer 1996, 37, 5375.
33. Broutman, L. J.; Bhatnagar, A.; Choi, S. Residual Stress Studies in Polyethylene Gas Pipes and Fittings, Final Report; GRI Contract 5082-271-0790545; GRI: Chicago, 1986.
34. Popelar, C. H.; Kenner, V. H.; Wooster, J. P. Polym Eng Sci 1991, 31, 1693.
35. Schultz, J. M. Polymer Materials Science; Prentice Hall: Englewood Cliffs, NJ, 1974; Chapter 11.
36. Young, R. J. Introduction to Polymers; Chapman & Hall: New York, 1981.
37. Kiass, N.; Chaoui, K. Rev Synth Sci Technol Annaba Univ 2002, 11, 25.
38. Marquez-Lucero, A.; G'Sell, C.; Neale, K. W. Polymer 1989, 30, 636.
39. Ashby, M. F.; Jones, D. R. H. Matériaux; Dunod Editeur: Paris, 1991; Vol. 2, Chapter 23.
40. Boyd, R. H. J Polym Sci Polym Phys Ed 1983, 21, 493.
41. Boyd, R. H. Polym Eng Sci 1979, 19, 1010.
42. Chudnovsky, A.; Shulkin, Y. Int J Fract 1999, 97, 83.
43. Ehrenstein, G. W.; Montagne, F. Matériaux Polymères: Structures, Propriétés et Applications; Hermes Science Publications: Paris, 2000; Chapter 6.
44. Chen, H.; Scavuzzo, R. J.; Srivatsan, T. S. J Mater Sci 1997, 16, 897.
45. Teoh, S. H.; Ong, E. H. Polymer 1995, 36, 101.
46. Ritchie, S. J. K.; Davis, P.; Leevers, P. S. Polymer 1998, 39, 6657.
47. Young, J. E.; Raphaelian, L. O.; Raske, D. T. Project Review Meeting; GRI Contract Number 5082-271-0717; GRI: Chicago, 1986.
48. Crist, B.; Fisher, C. J.; Howard, P. R. Macromolecules 1989, 22, 1709.
49. Boyd, R.; Liau, W. Macromolecules 1986, 19, 2246.
50. Brown, N. In Failure of Plastics; Brostow, W.; Corneliussen, R. D., Eds.; Hanser: New York, 1986; Chapter 6.
51. Peacock, A.; Mandelkern, L. J Polym Sci Part B: Polym Phys 1990, 28, 1917.
52. G'Sell, J.; Hiver, A.; Dahoun, A.; Souahi, A. J Mater Sci 1992, 27, 5031.
53. Hiss, R.; Hobeika, S.; Lynn, C.; Strobl, G. Macromolecules 1999, 32, 4390.
54. Hobeika, S.; Men, Y.; Strobl, G. Macromolecules 2000, 33, 1827.